



THE UNIVERSITY *of* EDINBURGH

Edinburgh Research Explorer

Surface Nanopatterning Using the Self-Assembly of Linear Polymers on Surfaces after Solvent Evaporation

Citation for published version:

Glynos, E, Chremos, A, Camp, PJ & Koutsos, V 2022, 'Surface Nanopatterning Using the Self-Assembly of Linear Polymers on Surfaces after Solvent Evaporation', *Nanomanufacturing and Metrology*, vol. 5, no. 3, pp. 297-309. <https://doi.org/10.1007/s41871-022-00152-8>

Digital Object Identifier (DOI):

[10.1007/s41871-022-00152-8](https://doi.org/10.1007/s41871-022-00152-8)

Link:

[Link to publication record in Edinburgh Research Explorer](#)

Document Version:

Peer reviewed version

Published In:

Nanomanufacturing and Metrology

General rights

Copyright for the publications made accessible via the Edinburgh Research Explorer is retained by the author(s) and / or other copyright owners and it is a condition of accessing these publications that users recognise and abide by the legal requirements associated with these rights.

Take down policy

The University of Edinburgh has made every reasonable effort to ensure that Edinburgh Research Explorer content complies with UK legislation. If you believe that the public display of this file breaches copyright please contact openaccess@ed.ac.uk providing details, and we will remove access to the work immediately and investigate your claim.



Surface Nanopatterning Using the Self Assembly of Linear Polymers on Surfaces after Solvent Evaporation

*Emmanouil Glynos,^{†, #, *} Alexandros Chremos,^{‡, %} Philip J. Camp,[‡] and Vasileios Koutsos^{†, **}*

[†]School of Engineering, Institute for Materials and Processes, The University of Edinburgh, Robert Stevenson Road, Edinburgh, EH9 3FB, United Kingdom

[‡]School of Chemistry, The University of Edinburgh, David Brewster Road, Edinburgh EH9 3FJ, United Kingdom

[#] Department of Materials Science and Technology, University of Crete, Heraklion 71003, Greece

[%]Present address: Section on Quantitative Imaging and Tissue Sciences, *Eunice Kennedy Shriver* National Institute of Child Health and Human Development, National Institutes of Health, Bethesda, Maryland 20892, USA

*E-mail: eglynos@iesl.forth.gr, eglynos@materials.uoc.gr (E. Glynos)

**E-mail: vasileios.koutsos@ed.ac.uk (V. Koutsos)

To whom correspondence should be addressed: E-mail: vasileios.koutsos@ed.ac.uk; Phone: +44 (0)131 6508704; or E-mail: eglynos@iesl.forth.gr, eglynos@materials.uoc.gr; Phone: +30 2810 391353

ABSTRACT. The morphology of linear polybutadiene physisorbed on freshly cleaved mica from a dilute polymer solution is investigated through atomic force microscopy. A fine structure study shows that the monolayer morphology in air (after rapid solvent evaporation) depends strongly on the molecular weight (M_w) of the linear polymer, the adsorbed amount, and the conformation adopted by the adsorbed polymer chains under good solvent conditions. The dependence of the observed polymer structure on M_w is most significant for samples with high surface density, where the intermolecular interactions among the adsorbed polymers are important. For high surface density, the adsorbed polymers tend to aggregate and minimize unfavorable contacts with air for different M_w samples, leading to an isotropic structural pattern. These structural phenomena with increasing surface density are

explained on the basis of the intermolecular interactions of the adsorbed polymers under good solvent conditions and after the abrupt solvent evaporation, corresponding to poor solvent conditions. The experimental observation is further discussed using the results obtained from molecular dynamics simulations of a simple coarse-grained model.

INTRODUCTION

Polymers can form monomolecular polymer layers (monolayers) on surfaces that can serve as ultra-thin soft coatings altering the bare surface properties. Depending on the physicochemical properties of the polymers used, the resulting polymer-modified surface can impart many new properties and have a wide range of interesting applications. Over the last decades, polymer monolayers have been used in diverse areas such as colloidal stability [1-3], surface nanopatterning [4-6], adhesion [7-9], and tribology [10-12]. They can be formed by chemisorption/grafting chains (strong anchoring by covalent bonds) or by physisorption (weak chain attachment by van der Waals interactions) on appropriate substrates where (in principle) all monomers of the chains can be adsorbed on the substrate in the same way.

End-grafted polymers on surfaces have been extensively studied by experiments. Under good solvent conditions, the physical picture of such monolayers is quite simple. With regard to the grafting density, two regimes can be distinguished [13]: at low grafting densities, each chain is isolated, occupying roughly a half-sphere with a radius comparable to the radius of gyration (“mushroom” regime); at high grafting densities, the chains stretch away from the surface to avoid overlaps, thereby forming a polymer “brush”. Nevertheless, an interesting line of investigation, which has attracted considerable interest over the last decade, is the behavior and resulting conformation of end-grafted chains when the solvent conditions change from good to poor (*e.g.*, adsorbed polymers on a surface exposed to air). In general, chains under poor solvent conditions will collapse to avoid contact with the solvent: at low grafting densities, the chains collapse independently from one another; at high grafting densities, the chains may collapse with others to form aggregates. These effects alter the polymer conformation and structure as compared with those under good solvent conditions.

With regard to experiments, the introduction of atomic force microscopy (AFM) allowed the direct imaging of single molecules, molecular assemblies, and polymer films in the dry state. Koutsos *et al.* [14, 15] studied the structural regimes of thiol-end-functionalized polystyrene (PS-SH) monolayers on gold substrates when the solvent quality changed from good to poor. Three different structural phases were observed on the basis of the grafting density. At low grafting densities, the chains collapsed individually, forming pancakes or small nanodroplets. At high grafting densities, which are high enough for chains to overlap with one another under good solvent conditions, the chains collapsed in groups and fused, forming surface-pinned micelles when the solvent conditions changed to poor (*i.e.*, upon evaporation of the good solvent). By performing adsorption under poor solvent conditions, high adsorbed amounts were achieved, and a third structural regime of laterally asymmetric structures (dense elongated islands) was observed. In all cases, the observed structures were driven by the effective monomer–monomer and chain–chain attractions that arose when the solvent conditions changed from good to poor. Siqueira *et al.* [16] studied polystyrene-block-polybutadiene functionalized with polar urazole groups and adsorbed onto silicon wafers. They achieved high grafting densities and observed homogeneous layers. The experimental observation of the behavior of grafted polymer chains under poor solvent conditions is consistent with theoretical and numerical predictions [17-24]. Sevick *et al.* [25], who used analytical theory and Monte Carlo computer simulations, extended the surface-pinned micelle problem to strongly adsorbing surfaces. Polymer attachment on the substrate surface occurs by end-tethering and monomer adsorption along the chain. They showed that tethered polymers on strongly adsorbing surfaces fuse together under poor solvent conditions, but such polymers formed compact globular micelles instead of pinned micelles.

Chains that are physisorbed by weak (*e.g.*, van der Waals) interactions on solid surfaces are not restricted by any tethers. Thus, although the experimental situation is simple, the resulting structure upon any change in solvent conditions or the evaporation of the solvent can be dramatic. The adsorption behavior and resulting conformation of linear physisorbed chains under good solvent conditions are comprehensively understood. The resulting conformations range from isolated chains (low adsorbed amounts) to relatively dense monolayers (high adsorbed amounts) [26, 27]. The conformation of a single/isolated physisorbed linear chain onto a weakly adsorbing surface is driven by the competition between the decrease in energy ($\Delta U < 0$) from binding monomers to the substrate and the loss of conformational entropy ($\Delta S < 0$). Although the binding energy is usually less than $k_B T$ per monomer in

contact with the surface, the net decrease in energy from forming many contacts outweighs the increase in free energy from the entropy change, $-T\Delta S > 0$ (which is of the order of $k_B T$). Consequently, the net free energy change of binding $\Delta F = \Delta U - T\Delta S < 0$. Hence, the chain tends to maximize the number of contacts with the substrate [27]. The conformation of a physisorbed homopolymer chain under good solvent conditions consists of the following motifs: *trains*, parts of the chain consisting of monomers that are in contact with the substrate; *loops*, parts of the chain having no contact with the surface and connecting two trains; *tails*, the non-adsorbed ends of the chain [26, 28]. The dimension of an adsorbed chain can be expressed with regard to its blob size. In general, an adsorption blob is defined as the length scale of a chain, in which the cumulative interaction energy is of the order of $k_B T$ (thermal energy). Using scaling arguments and assuming that the energy gain of the chain for an adsorbed monomer is $-\delta k_B T$ ($0 < \delta \ll 1$ for the case of weak adsorption), the adsorption blob size (ξ_{ads}) is [27]:

$$\xi_{\text{ads}} \approx \frac{b}{\delta^{v/(1-v)}} \quad (1)$$

where b is the Kuhn segment size, and v is the Flory scaling exponent that denotes the quality of the solvent. v can adopt one of three values, $3/5$, $1/2$, and $1/3$ in an athermal (good) solvent, θ -solvent, and poor solvent, respectively. Equation 1 shows that in the case of a single isolated chain, the blob size (and hence the thickness of the adsorbed chain) is independent of the number of monomers and consequently is also independent of the molecular weight of the polymer chain. When many chains are adsorbed on a surface under good solvent conditions, the adsorption and resulting structure for each polymer chain are influenced by the effective repulsive interactions with the surrounding adsorbed chains. In this case, the length of the tails and loops depends on the polymer concentration adsorbed on the surface and the chain length (related to M_w) [26]. The Scheutjens–Fleer theory [29] predicts that for low surface coverage (small number of chains on the surface), the chains “flatten” on the surface to decrease the energy of the system, that is, the chains adopt small loops and tails. By increasing the surface coverage, the chains appear with longer loops and tails because of the excluded-volume interactions with the surrounding adsorbed chains. In the case of high adsorption, the tails are longer than the loops. Using scaling arguments, Semenov and Joanny [30] have shown that the outer structure of adsorbed polymer layers is dominated primarily by the tails of the adsorbed polymer chains rather than the loops. The average number of segments in the tail, and hence the tail length increases linearly with M_w . The effects of polydispersity on adsorption have also been reported [26]. When the adsorption of the polymer occurs from a dilute solution at equilibrium (final stages of adsorption), high-molecular-weight polymers adsorb preferentially over low-molecular-weight ones because the entropy of mixing in the solution

decreases strongly with the increase of chain length, thereby leading to the adsorption of longer molecules on the surface.

Few experimental studies on the behavior and resulting structures of weakly physisorbed polymer monolayers when the solvent conditions change from good to poor have been documented. Structural investigations of sub-monolayers and monolayers of regular star-shaped polybutadiene (PB) polymers physisorbed on mica surfaces by experiments [31] and simulations [32] have been reported. These studies revealed a strong connection between the structures under dry conditions and the conformational properties of these molecules under good solvent conditions. Given these observations, this work aimed to study the self-assembled patterns of linear homopolymer PB chains physisorbed on mica; the mechanical and wetting properties of individual linear homopolymer PB nanodroplets have been studied previously [33, 34]. This system provides us the opportunity to discuss the fundamental aspect of linear-chain physisorption under good solvent conditions and to reveal the adsorbed polymer chain collapse and clustering behavior when the solvent conditions change. Furthermore, it demonstrates a facile method for the formation of isotropic and hierarchical nanopatterns on surfaces. It also complements the experimental star polymer study [31] and shows the differences in the observed structures when the number of arms is only two (*i.e.*, linear polymer chains). This study used three molecular weights, and it focused on two key dependencies: the effects of the surface density and the molecular weight on the observed nanostructures and patterns. The results demonstrate the existence of self-organized structures with characteristic distances among the aggregates. The molecular-scale origin of the observations is discussed and compared with other polymer architectures and fabrication protocols. To the best of our knowledge, this study is the first to perform an experimental comparison for the same chemical system (in our case, PB on mica), revealing some surprising differences and similarities. Finally, the interpretation of the results is supported by molecular dynamics (MD) simulations of a simple coarse-grained model.

EXPERIMENTAL AND SIMULATION METHODOLOGY

Materials. Linear PB polymer chains of three different molecular weights were used (Table 1); the polymers were dissolved in an appropriate volume of toluene so that the corresponding polymer solutions were at concentrations

below the critical overlap concentration (c^*). In this work, $c/c^* \approx 0.3$. Toluene was used as received (Fisher Scientific, Loughborough, UK). Mica (Agar Scientific, Essex, UK) was cleaved before being used.

Table 1: Linear PB molecular characteristics

M_w (kg/mol) ^a	M_w/M_n ^b	R_g (nm) ^c	V_{molecule} (nm ³) ^d	R_b (nm) ^e
38.6	1.03	7.74	72	2.58
78.8	1.05	11.9	147	3.27
962	1.1	53.3	1795	7.54

^a M_w , weight average molecular weight; ^b M_n , number average molecular weight; ^c R_g , radius of gyration under dilute good solvent conditions from light scattering measurements [35, 36]; ^d V_{molecule} , calculated volume of a collapsed molecule (based on the molecular weight and bulk density of PB, $\rho = 0.89 \text{ g/cm}^3$ [27]); ^e R_b , calculated radius under poor solvent conditions (compact sphere, using the bulk PB density)

Preparation of Linear PB Monolayers on Mica. All samples were prepared by exposing freshly cleaved mica to a toluene solution (good solvent for PB) with a desired concentration of the linear PB with $c < c^*$. Different incubation time periods were used: 2, 5, and 10 min for $M_w = 38.6 \text{ kg/mol}$; 2, 5, and 30 min for $M_w = 78.8 \text{ kg/mol}$; and 5, 10, and 60 min for $M_w = 962 \text{ kg/mol}$. In all cases, the mica surface was removed from the solution, placed in a 100 mL toluene bath for 24 h, and then rinsed exhaustively with 100 mL of toluene. The samples were dried gently under a nitrogen stream. All samples were imaged in air by AFM in tapping mode.

Atomic Force Microscopy (AFM). All experiments were conducted using a PicoSPM (Molecular Imaging and Agilent Technologies) operating in tapping mode in air. Commercially available Si_3N_4 rectangular cantilevers (MikroMasch, Tallinn, Estonia) with a spring constant of 1.75 N/m and resonance frequency of 130–160 kHz were

used. The cantilevers oscillated 5% below their natural resonant frequency and moved in a raster fashion during imaging. Each sample was imaged over several different areas.

Convolution Effect. The AFM tip can cause an object lying on a surface to appear wider because of the convolution of the geometry of the tip and the shape of the object being imaged. In a previous publication [31], the influence of tip geometry on the apparent dimension of an object being imaged with AFM has been discussed. Using similar geometrical arguments and assuming that the object is a spherical cap (as this has been shown to be a reasonable assumption for the case of linear polymer molecules on surfaces under poor solvent conditions [14, 37]), the real volume (V_r) of the object imaged can be estimated with regard to the apparent height (h), apparent volume (V_a), and radius of the tip (R_t) using the following relation:

$$V_r = V_a - \pi h^2 R_t \quad (2)$$

All tips used for the experiments were imaged through scanning electron microscopy, and the measured tip radii were in the region of 50 nm. However, this type of simple deconvolution is approximate, and estimated deconvoluted volumes can be 100% or even 200% larger than the real volume of the object imaged [37]. Thus, precise quantitative measurements of chain volumes are difficult to obtain. Nevertheless, these calculations can provide the order of magnitude of real volumes and helped us to determine whether or not the observed structures represent single collapsed molecules by comparing calculated molecular volumes with the observed convoluted volumes.

Island Volumes and Height Calculations. All images are shown without any image processing except for horizontal leveling using WSxM [38]. The height distribution of polymer islands was determined by performing grain analysis in Scanning Probe Image Processor (SPIP, Image Metrology, Hørsholm, Denmark). The total adsorbed amount, Γ (mg/m²), was calculated by adding all the deconvoluted volumes of polymer islands and using the bulk PB density. Notably, the abovementioned analysis was performed for AFM images corresponding to the samples prepared using linear PB with M_w of 78.8 and 962 kg/mol. In the case of the linear PB with M_w of 38.6 kg/mol, the analysis was restricted to the height measurement of particles through their cross-section profiles. At a low molecular weight, the volumes of the islands were difficult to determine, as the small size of the molecules (particularly in the xy plane) interfered with the background noise level of the AFM image, thereby hindering the

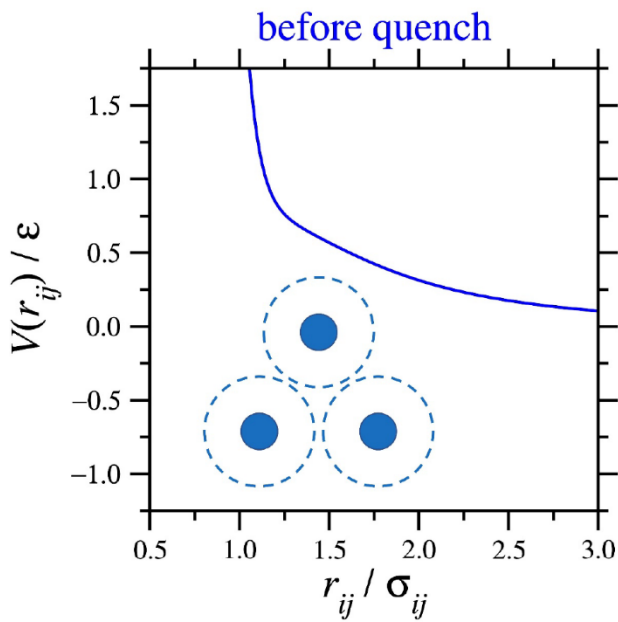
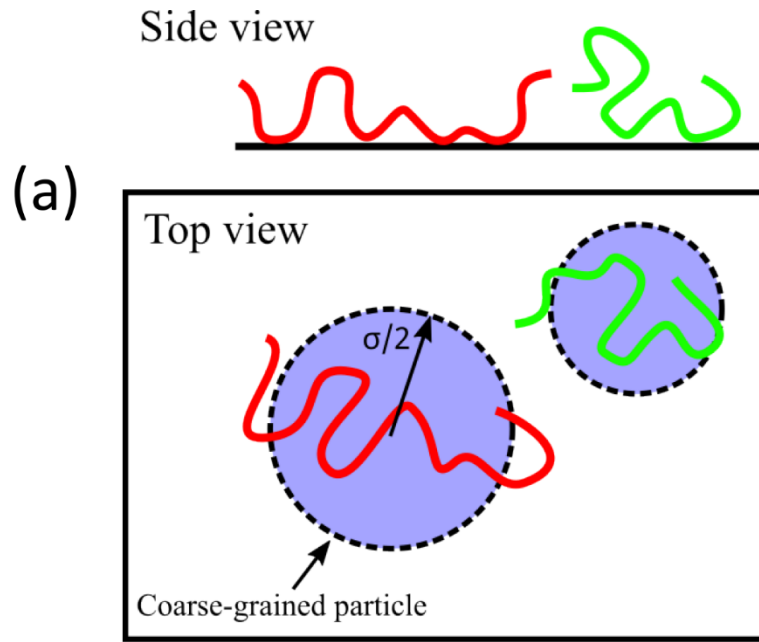
accurate application of the grain analysis module of SPIP. For these samples, the corresponding adsorbed amount was measured using the roughness analysis module (height distribution of pixels) of SPIP, which corresponds to the convoluted adsorbed amount of the samples. Therefore, these measurements can provide only qualitative information on the adsorbed amount of the corresponding samples.

Simulation Methodology. MD simulations of a coarse-grained model have been performed to obtain insight into the experimental results and understand the clustering phenomena. The aim was to understand how the polymer surface density gives rise to different cluster distributions and how a bimodal distribution might arise. Although a bead-spring model has been used previously [39], providing valuable insights, here we attempt to investigate the clustering phenomena at hand by simplifying the model. Thus, a two-dimensional coarse-grained model was adopted; each chain molecule adsorbed on the surface is represented by a single particle (Figure 1a). This is a simplification, but with appropriate parameterization, it can describe the good-to-poor solvent quench. Under good solvent conditions, the polymers experience a net, mutual repulsion, which has been shown explicitly for self-avoiding polymer chains in bulk solution [40]. Two coarse-grained polymer particles, i and j , are confined to two dimensions, and they interact via a pair potential, $V(r_{ij})$, given by a sum of Lennard–Jones (LJ) and repulsive terms.

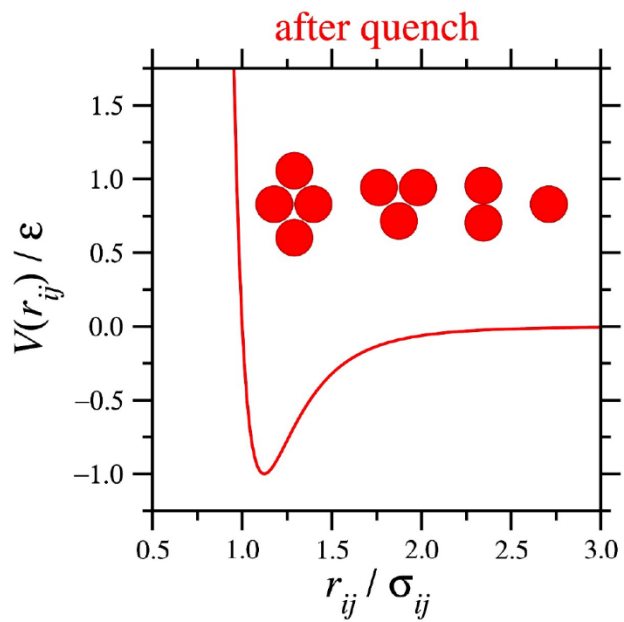
$$V(r_{ij}) = \begin{cases} 4\varepsilon \left[(\sigma_{ij}/r_{ij})^{12} - (\sigma_{ij}/r_{ij})^6 \right] + \varepsilon' (\sigma_{ij}/r_{ij})^3; & r_{ij} < 3\sigma_{ij} \\ 0; & r_{ij} \geq 3\sigma_{ij} \end{cases} \quad (3)$$

Here ε is the depth of the LJ potential (assumed equal for all pairs), $\sigma_{ij} = (\sigma_i + \sigma_j)/2$ is the range parameter with regard to the diameter of particles, and r_{ij} is the separation between the two particles in the plane. The parameter ε' controls the strength of an additional repulsive potential term. This repulsive term is utilized to describe the different solvent conditions: under good solvent conditions, the overall interaction should be repulsive (Figure 1b). Thus, we selected $\varepsilon' = 3\varepsilon$. Under poor solvent conditions, the total interaction should include a short-range attraction (Figure 1c), which is achieved by setting $\varepsilon' = 0$ and leaving only the Lennard–Jones contribution. The additional repulsive term is not a rigorous result for polymers, and it is only introduced to mimic the long-range repulsion, which is entropic in origin, between chains under good solvent conditions. In order to represent polymer polydispersity, systems of $N = 2500$ particles were prepared with Gaussian-distributed mass distribution, $p(m)$, with a mean value $\bar{m} = 1$, and a variance was selected to match the average experimental value ($M_w/M_n = 1.05$). The

corresponding diameters were obtained using $\sigma \propto \sqrt{m}$ and scaled to an average value $\bar{\sigma} = 1$. All calculations were performed in a square simulation cell under periodic boundary conditions using a linked cell scheme. Standard MD simulations were performed in the canonical ensemble using the Gaussian isokinetic thermostat [41]. The equations of motion were integrated using the leapfrog algorithm with a reduced timestep of $0.05\sqrt{m\bar{\sigma}^2/\epsilon}$.



(b)



(c)

Figure 1. Schematic diagram illustrating the simulation of the two-dimensional coarse-grained models of polymer cluster formation upon solvent evaporation (the “quench”). (a) Each polymer is modeled as a structureless particle. (b) Before the quench, the particles are in good solvent conditions, and the net interaction is repulsive. This is modeled using the Lennard–Jones potential plus a strong r_{ij}^{-3} repulsion, with the latter just being a device to prohibit clustering. A configuration of particles is shown, where the solid core is the post-quench particle size (one unit), and the dashed circle is the pre-quench repulsion range (three units). (c) After the quench, the particles are in poor solvent conditions, making the net interaction attractive. This is modeled by turning off the r_{ij}^{-3} repulsion. The particles can cluster, and they can be stabilized by the attractive well in the Lennard–Jones potential. A range of cluster sizes is anticipated.

The size of the simulation box was adjusted to cover a range of adsorbed amounts of polymer (with the total number of polymers N held fixed): the smaller the box, the longer the incubation time, and the higher the adsorbed amount. The simulation protocol was as follows: particles were equilibrated at the desired surface density to simulate the system in good solvent conditions ($\varepsilon' = 3\varepsilon$), as measured by $\rho^* = N\bar{\sigma}^2/A$, where A is the area of the simulation cell. In addition, the interaction potential was modified by setting $\varepsilon' = 0$ to mimic the effects of abrupt solvent evaporation and the resulting crossover to poor solvent conditions; the remaining LJ potential has a short-range attractive well, which mimics the net and mutual attractions experienced by polymers under poor solvent conditions. Clusters were identified using a distance-based cutoff of $1.8\bar{\sigma}$. Simulations were performed over a wide range of surface densities. For a given surface density, six simulations were performed with different sets of particle diameters drawn from the appropriate diameter distribution, and the results were averaged.

RESULTS

For each polymer used, several samples using different adsorption/incubation times were prepared. Figures 2a, 2b, and 2c show typical AFM height images of linear PB with $M_w = 38.6$ kg/mol adsorbed on a freshly cleaved mica for three different adsorbed amounts (shown at the top of each image). Analyzing several images for each adsorbed amount, we obtained the corresponding height histograms of the polymer islands (Figures 2d, 2e, and 2f).

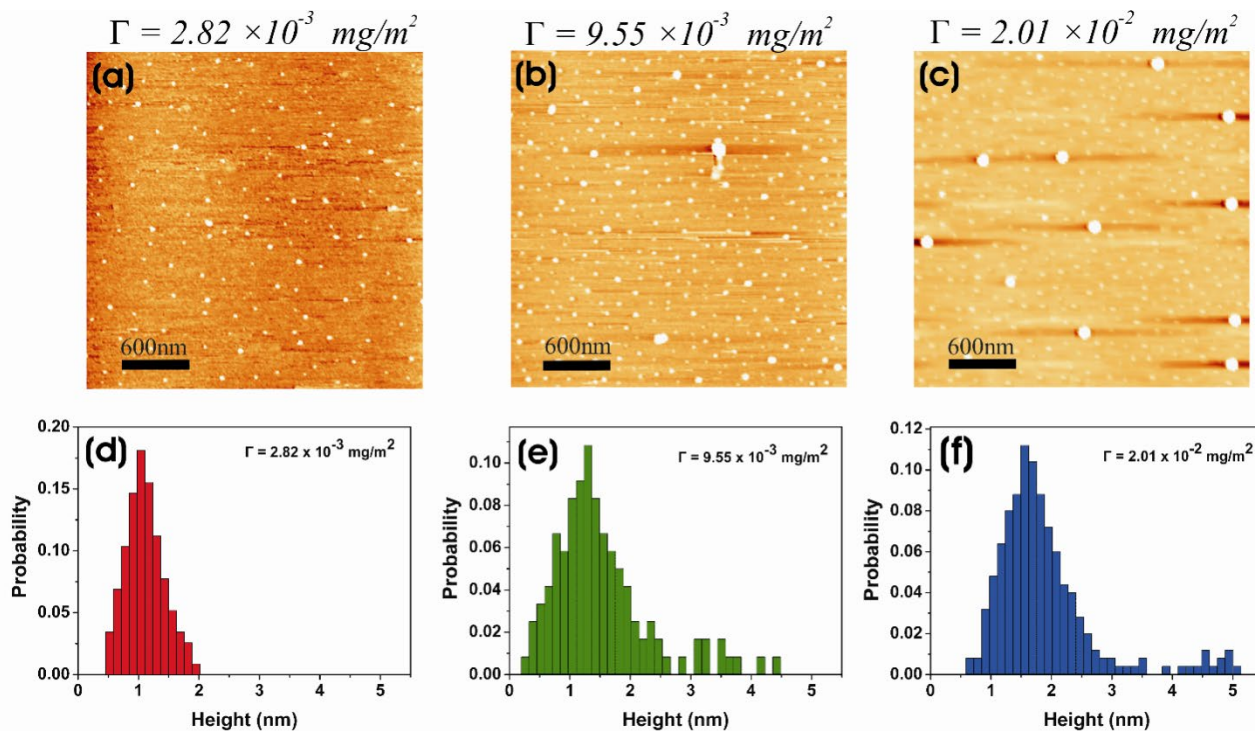


Figure 2. (a–c) Tapping mode AFM height images ($3 \mu\text{m} \times 3 \mu\text{m}$) and (d–f) the total distribution of the island height of a freshly cleaved mica exposed to linear PB solution with $M_w = 38.6 \text{ kg/mol}$ for different adsorbed amounts; (a) and (d) correspond to an adsorbed amount of $\Gamma = 2.82 \times 10^{-3} \text{ mg/m}^2$; (b) and (e) correspond to $\Gamma = 9.55 \times 10^{-3} \text{ mg/m}^2$; (c) and (f) correspond to $\Gamma = 2.01 \times 10^{-2} \text{ mg/m}^2$.

Figure 2a corresponds to low incubation time, and hence low adsorbed amount (PB with $M_w = 38.6 \text{ kg/mol}$ and $\Gamma = 2.82 \times 10^{-3} \text{ mg/m}^2$); the polymer islands appear flat (short) and circular. The chains took the globular conformation because the imaging took place in air (*i.e.*, poor solvent conditions result in collapsed chains). The height distribution of the islands (Figure 2d) is nearly symmetric, with a small tail at larger heights and a clear peak at approximately 1.0 nm. As the adsorbed amount increased (Figure 2b; $\Gamma = 9.55 \times 10^{-3} \text{ mg/m}^2$), the number and size of polymer islands increased; they are higher than those observed during short incubation time periods. The height distribution (Figure 2e) maintains a nearly symmetric part with a peak at approximately 1.3 nm, but some higher islands (3.0–4.5 nm) started to appear, corresponding to the large islands evidently observed in the corresponding AFM image. For the highest adsorbed amounts studied here, $\Gamma = 2.01 \times 10^{-2} \text{ mg/m}^2$ (Figure 2c), the number of islands increased further, and large islands that were observed at intermediate adsorbed amounts

increased in size. The height distribution of the islands (Figure 2f) has a nearly symmetric part with a peak at approximately 1.7 nm and a “tail” of islands with a height of 3.8–5.1 nm.

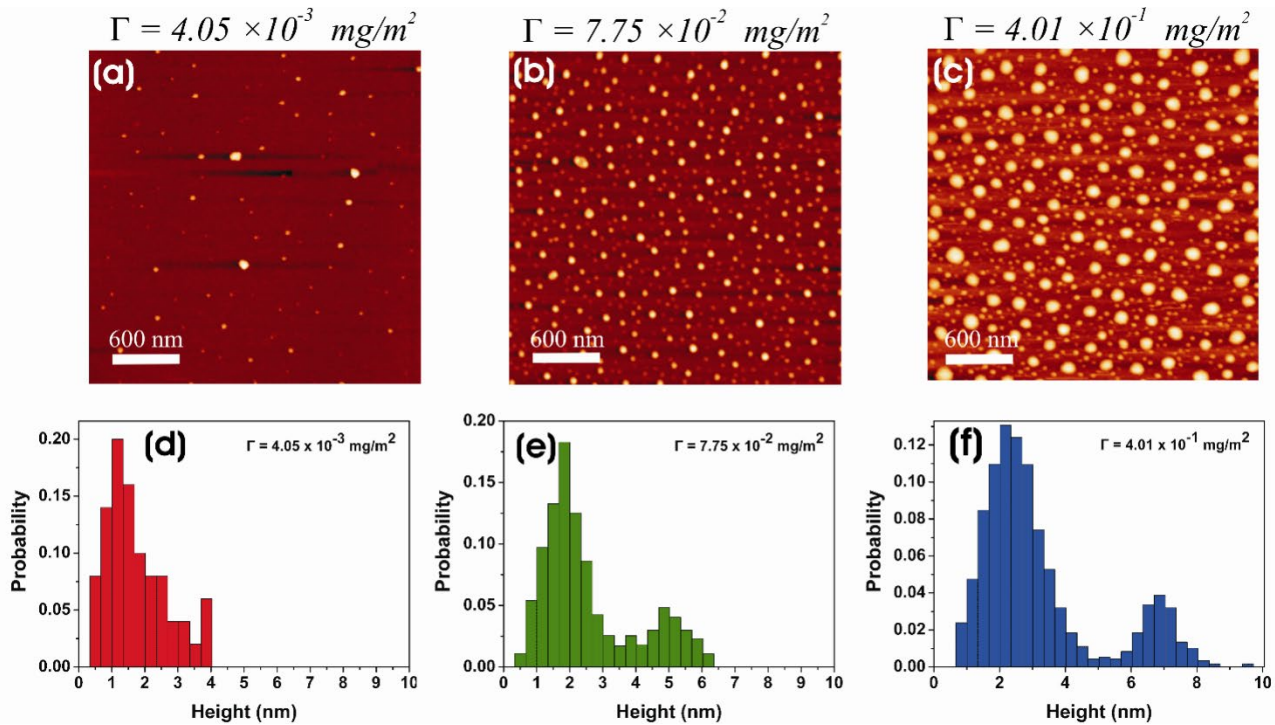


Figure 3. (a–c) Tapping mode AFM height images ($3 \mu\text{m} \times 3 \mu\text{m}$) and (d–f) the total distribution of the island height of a freshly cleaved mica exposed to linear PB solution with $M_w = 78.8 \text{ kg/mol}$; (a) and (d) correspond to $\Gamma = 4.05 \times 10^{-3} \text{ mg/m}^2$; (b) and (e) correspond to $\Gamma = 7.75 \times 10^{-2} \text{ mg/m}^2$; (c) and (f) correspond to $\Gamma = 4.01 \times 10^{-1} \text{ mg/m}^2$.

Figures 3a, 3b, and 3c present typical AFM images of the linear PB with $M_w = 78.8 \text{ kg/mol}$ adsorbed on mica for three different incubation time periods, which correspond to different adsorbed amounts. In Figure 4, we present some high-contrast, zoom-in AFM images. For a low adsorbed amount $\Gamma = 4.05 \times 10^{-3} \text{ mg/m}^2$, the islands are flat on the surface (short) and circular, as in the case of $M_w = 38.6 \text{ kg/mol}$. Increasing the adsorbed amount, $\Gamma = 7.75 \times 10^{-2} \text{ mg/m}^2$, the number of islands increased, and larger islands started to appear (Figure 3b and the zoom-in Figure 4a). For high adsorbed amounts, $\Gamma = 4.01 \times 10^{-1} \text{ mg/m}^2$, larger islands were formed (Figure 3c or zoom-in Figure 4b). In all cases, polymer islands remained circular.

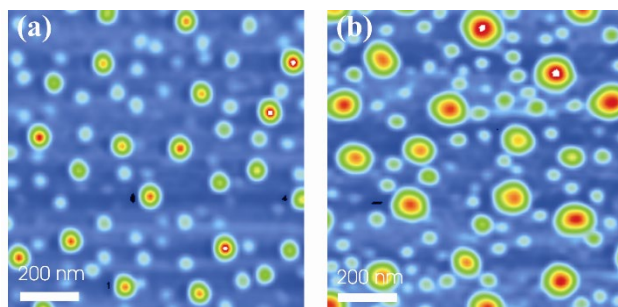


Figure 4. High-contrast AFM images in air of linear PB solution with $M_w = 78.8$ kg/mol, $1 \mu\text{m} \times 1 \mu\text{m}$. Image (a) corresponds to the adsorbed amount of $\Gamma = 7.75 \times 10^{-2}$ mg/m², and (b) corresponds to $\Gamma = 4.01 \times 10^{-1}$ mg/m².

For $\Gamma = 4.05 \times 10^{-3}$ mg/m², the height histogram has a peak at approximately 1.2 nm and a small secondary peak at approximately 3.8 nm (Figure 3d). The polymer islands with a height up to 3.5 nm correspond to single collapsed polymer chains, as the average deconvoluted volume of these islands is 274 nm³, which is of the same order as the one calculated on the basis of the molecular weight and bulk density (Table 1). The islands with a height of approximately 3.8 nm (corresponding to the secondary peak) occupy volumes of approximately 400 nm³, which can be considered as aggregates of around two polymer chains. Increasing the adsorbed amount to $\Gamma = 7.75 \times 10^{-2}$ mg/m², the height distribution of the polymer islands obtained a bimodal character, with the first peak at 1.8 nm and the second peak at 5.0 nm (Figure 3e). For a higher adsorbed amount, $\Gamma = 4.01 \times 10^{-1}$ mg/m², the height distribution of the polymer islands maintained a clear bimodal characteristic with the first peak at 2.2 nm and the second peak at 7.0 nm.

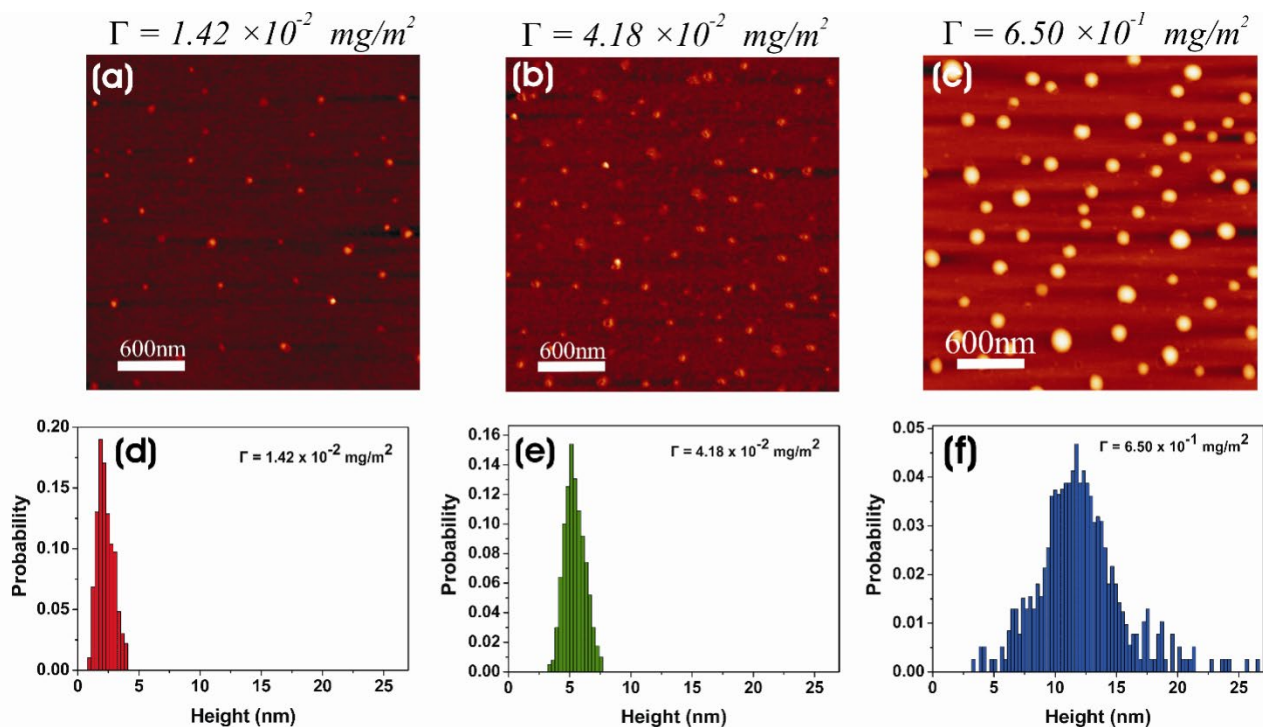


Figure 5. (a–c) Tapping mode AFM height images ($3 \mu\text{m} \times 3 \mu\text{m}$) and (d–f) the total distribution of the island height of a freshly cleaved mica exposed to linear PB solution with $M_w = 962 \text{ kg/mol}$; (a) and (d) correspond to an adsorbed amount of $\Gamma = 1.42 \times 10^{-2} \text{ mg/m}^2$; (b) and (e) correspond to $\Gamma = 4.18 \times 10^{-2} \text{ mg/m}^2$; (c) and (f) correspond to $\Gamma = 6.50 \times 10^{-1} \text{ mg/m}^2$.

In Figure 5, we present typical AFM images of linear PB with $M_w = 962 \text{ kg/mol}$ adsorbed on mica for three different adsorbed amounts. For a low adsorbed amount, $\Gamma = 1.42 \times 10^{-2} \text{ mg/m}^2$, the polymer islands appeared flat (short) on the surface and circular. For an intermediate adsorbed amount, $\Gamma = 4.18 \times 10^{-2} \text{ mg/m}^2$, the number of islands increased. For a high adsorbed amount, $\Gamma = 6.50 \times 10^{-1} \text{ mg/m}^2$, large circular polymer islands appeared. In all cases, polymer islands remained circular.

For low adsorbed amount, $\Gamma = 1.42 \times 10^{-2} \text{ mg/m}^2$, the height distribution of the polymer islands appears nearly symmetric with a peak at approximately 1.8 nm (Figure 5d). In this case, all the polymer islands correspond to single collapsed chains because their average deconvoluted volume of approximately 3000 nm^3 is comparable to the one calculated on the basis of the molecular weight and bulk density (Table 1). For an intermediate adsorbed amount, $\Gamma = 4.18 \times 10^{-2} \text{ mg/m}^2$, the height distribution remains nearly symmetric, but the peak shifts upwards to

approximately 5.2 nm (Figure 5e). Similarly, the polymer islands correspond to single collapsed polymer chains, as their average deconvoluted volume is still 3000 nm³. For a high adsorbed amount, $\Gamma = 6.50 \times 10^{-1}$ mg/m², the height distribution of the polymer islands retained its nearly symmetrical shape, but the distribution peak further increased to approximately 12 nm (Figure 5f). In this case, the polymer islands correspond to aggregates of several polymer chains because the deconvoluted volume of the polymer islands is larger than the theoretical volume of the single collapsed chain.

As shown in Figure 6, the average radial distribution of the 2D fast Fourier transform (FFT) was considered for the patterns obtained for the highest adsorbed amounts in the case of linear PB with $M_w = 78.8$ kg/mol (Figure 6, top) and $M_w = 962$ kg/mol (Figure 6, bottom). In general, if the shape of an FFT is centrosymmetric, then the surface pattern is isotropic. The average radial distribution of a centrosymmetric FFT shows a clear maximum at a specific wave number $q = 1/\lambda$ corresponding to a characteristic length scale λ , which is the preferred/characteristic distance of undulation/particles. In the case of $M_w = 78.8$ kg/mol and higher adsorbed amount ($\Gamma = 4.01 \times 10^{-1}$ mg/m²), the 2D FFT is centrosymmetric, and a maximum radial average intensity can be observed at $q \approx 4.52 \mu\text{m}^{-1}$, which corresponds to a characteristic distance of $\lambda = 221$ nm (Figure 6, top). In the case of linear PB with $M_w = 962$ kg/mol and for the highest adsorbed amount ($\Gamma = 6.50 \times 10^{-1}$ mg/m²), a clear centrosymmetric 2D FFT can be observed with a maximum radial average intensity at $q \approx 2.34 \mu\text{m}^{-1}$, indicating a characteristic distance of $\lambda = 427$ nm (Figure 6, bottom).

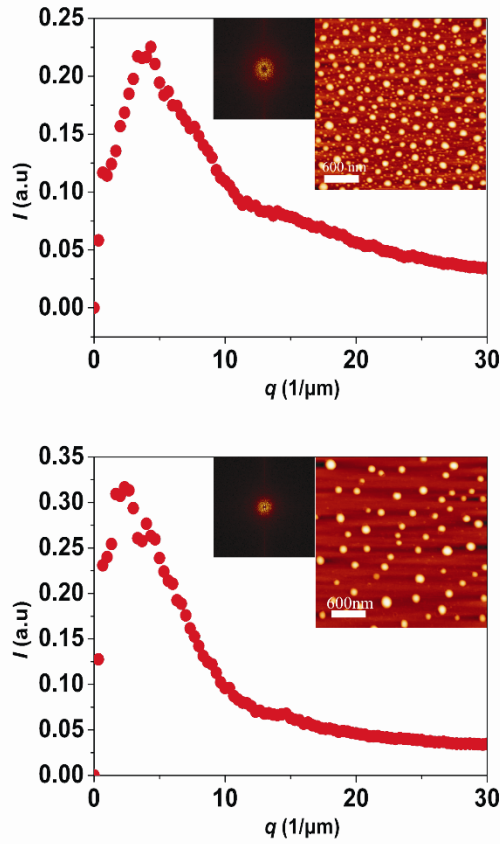


Figure 6. Relative average intensity (I) as a function of the wave number ($q = 1/\lambda$) for linear PB of (top) $M_w = 78.8$ kg/mol and $\Gamma = 4.01 \times 10^{-1}$ mg/m² and (bottom) $M_w = 962$ kg/mol and $\Gamma = 6.50 \times 10^{-1}$ mg/m². The characteristic distances from top to bottom are 221 and 427 nm, respectively. Insets show the AFM image and corresponding 2D-FFT.

DISCUSSION

In all cases, after the abrupt solvent evaporation, the adsorbed chains collapsed individually or fused together to form aggregates. When the solvent conditions changed from good to poor, the system decreased the free energy by minimizing the unfavorable contact with air and forming globules/nanodroplets. The number and size of the globules increased with the incubation time of the substrate in the polymer solution. The observed patterns showed a strong dependence on the adsorbed amount and on the molecular weight of the adsorbed chains.

With regard to the molecular weights used ($M_w = 38.6, 78.8,$ and 962 kg/mol) and the smallest observed adsorbed amounts ($\Gamma = 2.82 \times 10^{-3}$ mg/m², 4.05×10^{-3} mg/m², and 1.42×10^{-2} mg/m², respectively), the vast majority of

polymer islands correspond to single collapsed linear chains. However, the presence of a minority of small aggregates cannot be excluded. This finding is certainly true in the case of $M_w = 78.8$ kg/mol, where the distribution of polymer islands in the lowest observed amount included some aggregates (as noted in the Results section, Figure 3d). The height of a single collapsed chain depends weakly on M_w . This result is illustrated in Figure 7, where the height of a single collapsed chain is plotted as a function of molecular weight. For the lowest observed adsorbed amounts, the island height increased by a factor of less than two (from 1.04 to 1.84 nm), although M_w was increased by almost two orders of magnitude. The number of adsorbed chains is similar in each case, which are 16 ± 3 , 15 ± 2 , and 5 ± 1 chains/ μm^2 for samples with $M_w = 38.6$, 78.8, and 962 kg/mol, respectively. In all cases, assuming that the adsorbed polymer chains were homogeneously and isotropically distributed on the surface when under good solvent conditions and before the abrupt solvent evaporation, the average distance between the centers of the molecules is between 250 and 300 nm. The chain–chain distance is higher than their radius of gyration when under good solvent conditions (Table 1). Hence, the interactions among adsorbed polymer chains are weak, and the adsorbed chains were isolated from one another.

As previously mentioned, the adsorption blob size and consequently the effective height of a single isolated chain under good solvent conditions should be independent of M_w . The fraction of the non-adsorbed monomers of an adsorbed chain, Φ_{na} , is defined as the ratio of monomers not in contact with the surface over the total number of monomers of the adsorbed chain, which is similar to the study of star polymers [31]. In the case of single/isolated molecules adsorbed on mica under good solvent conditions, Φ_{na} is independent of M_w . This behavior is deduced clearly from our experiments, although our measurements are in a dry state. In addition, the chains are in poor solvent conditions, which collapsed after the abrupt solvent evaporation. Single isolated chains collapsed with similar heights, almost independent of the molecular weight. Hence, our results indicate that the resulting height of the collapsed adsorbed chain is influenced critically by its conformational behavior when under good solvent conditions.

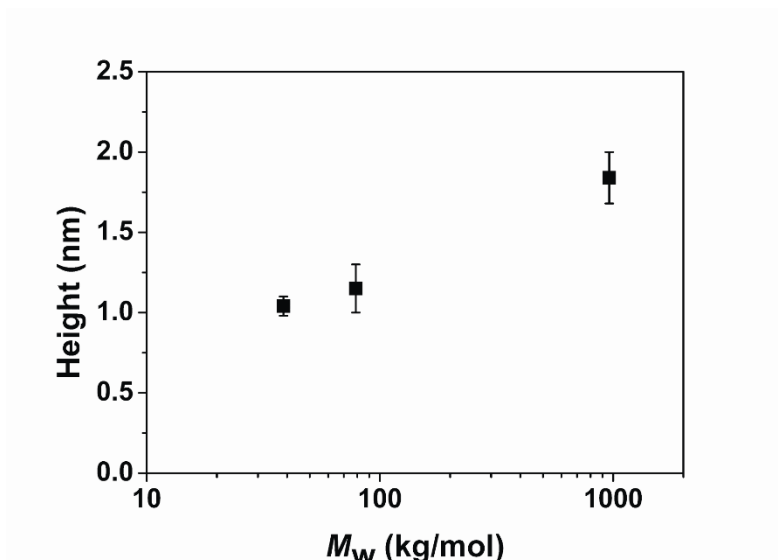


Figure 7. Semi-log plot of the height of the collapsed single chain against their M_w in the case of the lowest adsorbed amount.

With regard to the different molecular weights used in this study, the height of the islands consisting of single collapsed chains increased with the adsorbed amount, as shown in the peak of the distribution part that corresponds to single collapsed polymer chains (Figures 2, 3, and 5). For linear PB with $M_w = 38.6$ kg/mol, the height of the single collapsed chain increased gradually from 1.0 to 1.7 nm with the increase of the adsorbed amount. In addition, the linear PB with $M_w = 78.8$ kg/mol increased from 1.2 to 2.2 nm, and the linear PB with $M_w = 962$ kg/mol increased from 1.8 to 5.2 nm. As previously mentioned, the adsorption blob size and consequently the effective height of a single isolated chain under good solvent conditions should be roughly independent of molecular weight. However, an increase in the adsorbed amount led to chain “crowding” on the surface and thus to an increase of the repulsive interactions among the chains, which then adopted longer loops and tails. Consequently, the chain conformation is higher when under good solvent conditions. This behavior is also manifested in our measurements even when the chains are under poor solvent conditions; the chains collapse after the abrupt solvent evaporation. The volume of the single collapsed chain globule is fixed (the volume of a single chain), and imaging is performed at room temperature, which is well above the glass-transition temperature of PB. Thus, the dimension of the chain would be roughly independent of the adsorbed amount or the conformation of the chain when under good solvent conditions. Nevertheless, our results indicate that on the single-chain scale, the resulting height of the collapsed

chain is influenced by the conformational properties of the chain when under good solvent conditions. When the adsorbed amount (or the number of adsorbed chains) is increased, Φ_{na} increases as interchain repulsive excluded volume interactions dominate and individual chains take conformations with higher loops and tails and hence a smaller number of trains. The chains collapsed while maintaining the segmental contacts with the surface, preserving the favorable adsorption energy, and forming globular nanodroplets, which seem to be “pinned” in metastable states. The mechanical and wetting properties of individual linear-polymer nanodroplets have been studied in detail in previous studies [33, 34].

In all cases (different M_w), the number of islands increased (higher surface density) with incubation time and hence adsorbed amount. The tendency of chains to fuse together and form homogeneous aggregates after the abrupt solvent evaporation is pronounced in the case of the intermediate and highest adsorbed amounts (Figures 2, 3, and 5). Nevertheless, at intermediate-to-high adsorbed amount, the observed patterns show a strong molecular weight dependence: for $M_w = 38.6$ kg/mol, few aggregates were observed; for $M_w = 78.8$ kg/mol, the number of aggregates increased, and a bimodal distribution was obtained; for $M_w = 962$ kg/mol, almost exclusively large aggregates were observed. In all cases, the height of the aggregates was higher than that of single collapsed chains. At the same molecular weight, the height of the aggregates slowly increased as the number of chains in the aggregate increased. Moreover, higher molecular weights produced larger/higher aggregates.

In general, entanglement among chains in high-concentration polymer solutions can occur if the molecular weight of the chains is above the entanglement molecular weight, M_e [27]. In the case of entanglement among adsorbed chains, the case is complicated as entanglements may appear primarily among non-adsorbed parts of the chains (loops and tails). However, the length (and the corresponding molecular weight) of these sub-chains is not easy to determine. Hence, although M_w of the whole adsorbed chain can be higher than the corresponding M_e , the molecular weight of the largest loops and tails, $M'_w (< M_w)$, could be smaller than M_e . For PB, $M_e \approx 2$ kg/mol [27], which is much smaller than M_w of different polymer chains used in this study. Considering that M'_w is a fraction of the total chain M_w , one may assume that the higher the M_w of the adsorbed chain, the more probable it is that M'_w is higher than M_e . Hence, longer adsorbed chains could make entanglements in a more efficient way between their non-adsorbed loops and tails. Based on our results, higher molecular weights produce higher aggregates. For the highest

adsorbed amount observed, the ratio of aggregates over the total number of islands increased with M_w : for $M_w = 38.6$ kg/mol, few aggregates were observed; for $M_w = 78.8$ kg/mol, the number of aggregates increased, and a bimodal distribution is obtained; for $M_w = 962$ kg/mol, almost exclusively large aggregates were observed.

The experiments revealed that for physisorbed polymer layers exposed to air, the aggregation behavior is strongly influenced by the polymer molecular weight and molecular conformations when under good solvent conditions. For the 38.6 kg/mol polymer and for the higher adsorbed amount, the vast majority of chains collapsed individually after the abrupt solvent evaporation. Similarly, as the molecular weight increased to 78.8 kg/mol and for the highest adsorbed amount, aggregates coexist with single collapsed polymer chains, whereas for the highest molecular weight used in this study (962 kg/mol) and for the highest adsorbed amount, the vast majority of the chains fused together forming aggregates; therefore, a gradual transition of the self-assembly behavior of the physisorbed polymer chains with the chain molecular weight, when the solvent conditions change from good to poor, was established. This behavior is due to the fact that longer chains on a substrate adopt conformations with longer loops and tails compared with shorter chains. In this case, longer chains can make entanglements with the surrounding adsorbed polymers, and when the solvent conditions change from good to poor, attractive short-range interactions among the monomers bring them together to form larger aggregates, thereby minimizing their unfavorable contacts with air.

Simulations. Figure 8 shows the results of our simulations, indicating that the proportion and typical size of aggregates coexisting with isolated particles increase with the increase of surface density. Figure 8a shows a snapshot at low surface concentration. Each particle represents one polymer molecule, and almost no clustering of particles is observed. Figure 8c shows the corresponding cluster size distribution, which is unimodal, Gaussian, and centered on unit mass based on the underlying particle-size distribution. This finding indicates that most particles are not part of a cluster; a small number of clusters are observed occasionally, but they do not significantly affect the cluster distribution. The results at higher surface coverage are very different. Figure 8b shows that most particles are part of a cluster and that isolated particles are primarily small ones. Figure 8d shows the corresponding cluster-mass distribution. This function is bimodal, with a low-mass peak corresponding to isolated particles and a high-mass peak corresponding to clusters.

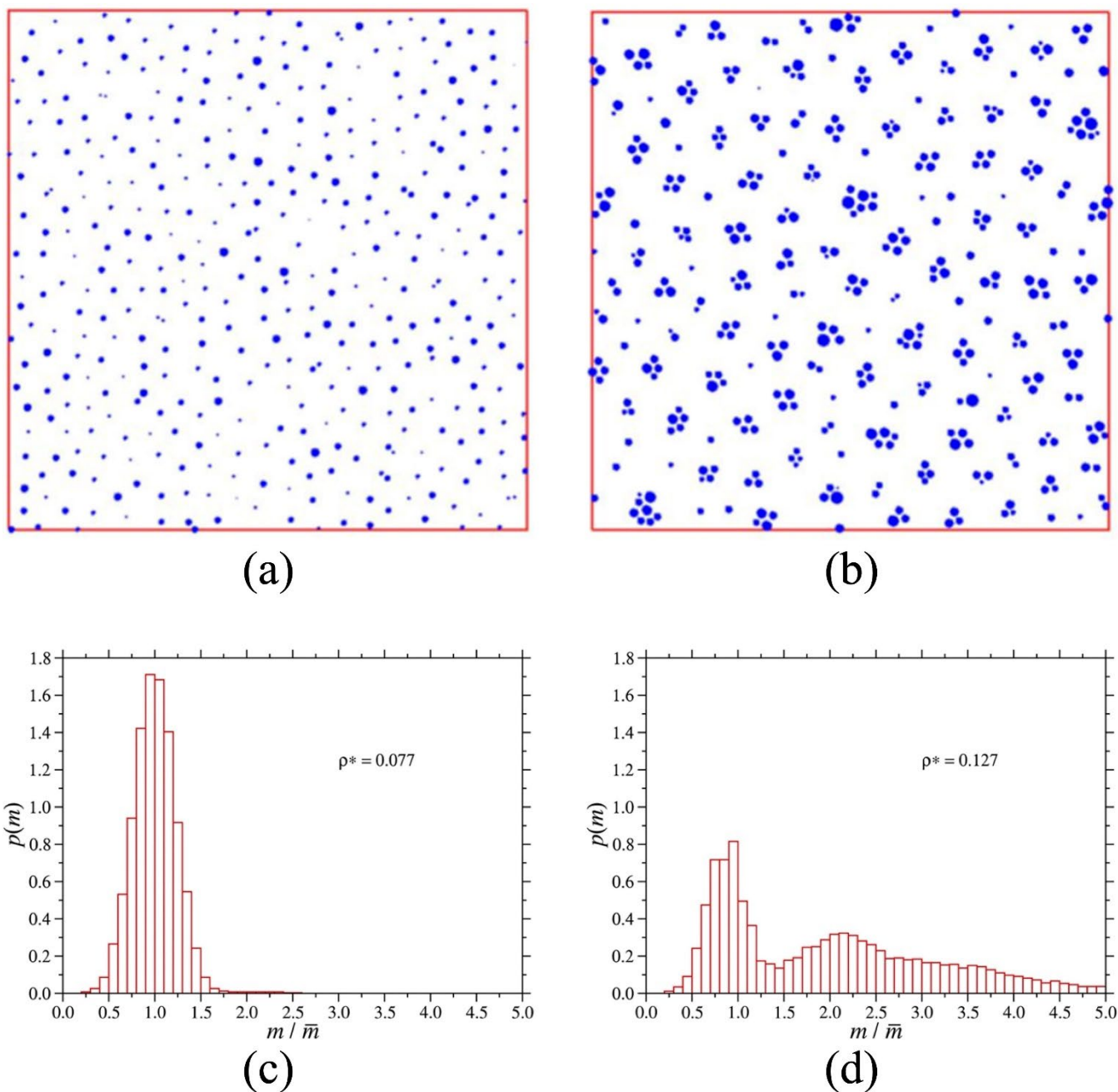


Figure 8. (a), (b) Snapshots of a system of 400 particles taken after 200,000 time steps at $\rho^* = 0.077$ and 0.127, respectively. (c), (d) Mass distributions from the simulation of 2500 particles at $\rho^* = 0.077$ and 0.127, respectively. For visualization purposes, (a) and (b) display only a small portion of the system. In (c) and (d), the mass is relative to the average particle mass.

Figure 9 supports the idea that the longer a polymer is, the more likely it is to cluster. In particular, the average mass of isolated chains—single particles in the case of these simulations—decreases with the increase in density,

which indicates that smaller chains are less likely to cluster. On the contrary, the average mass of clusters increases steadily with the increase in density. This finding indicates that at low densities, the longest chains will have a high tendency to cluster, but as density increases, intermediate-length chains will start to cluster, thereby reducing the average mass of single chains. At higher densities, $\rho^* > 0.11$, the average cluster mass increases, showing the growth of existing clusters.

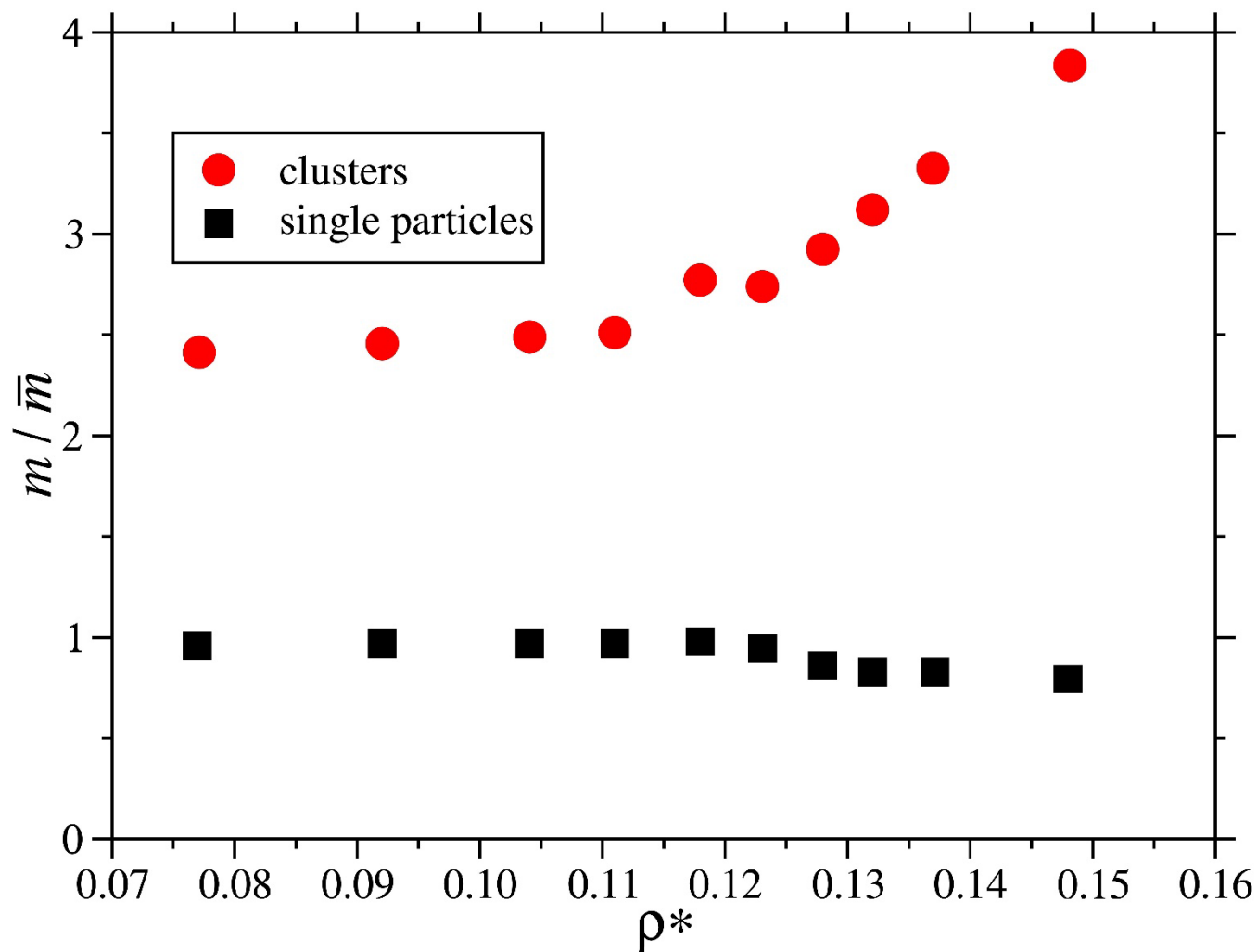


Figure 9. Average mass of clusters (red discs) and isolated polymers (black squares) at different densities. The mass is relative to the average particle mass.

Comparisons with Star Polymers and Spin-Coated Samples. As shown in Figure 6, for linear PBs with $M_w = 78.8$ and 962 kg/mol and for the highest observed adsorbed amounts, the polymers acquired isotropic distributions revealing some medium/long-range ordering behavior. These results are consistent with the results presented on star PB on mica for samples prepared by using the same experimental protocol [31]; in this case, the star molecules

acquired an isotropic distribution on the surface for relatively high adsorbed amounts. Molecules with different functionalities resulted in different surface patterns. The rapid solvent evaporation in various polymers on the surfaces has not been shown to affect the position of the adsorbed molecules (producing frozen conformations in the dry state) [42-45]. When the surface structures of polymer-modified surfaces are driven from dewetting instabilities, the observed patterns are independent of molecular weight [46]. Some studies reported that the morphologies of the star-polymer films on surfaces were related to the conformation of chains before the abrupt solvent evaporation. Therefore, in the case of linear PB, the observed patterns on mica are in accordance with the equilibrium structures of adsorbed polymers under good solvent conditions, and the observed structures may not be driven by solvent dewetting. In the case of the highest observed amount of 78.8 and 962 kg/mol polymers, the characteristic distance of the pattern increased from 221 to 427 nm, respectively (Figure 6), showing a molecular-weight dependence in the observed surface structure. However, at the last stages of drying, the resulting capillary forces could play a role in the aggregation behavior, particularly when the polymer density is relatively high because of the affinity between the polymer and solvent. Nevertheless, computer simulations of coarse-grained bead-spring models of linear [39] and star polymers [32], which mimic the effects of good-to-poor solvent conditions but do not consider the evaporation effects, support the hypothesis that the structures observed experimentally after quenching are correlated with the structures of polymers when under good solvent conditions.

Finally, the shapes of linear chains and star nanostructures on the surface were compared: [31] First, the shape of single-linear-chain globules is a symmetric spherical cap, which is quite different from the lowest functionality star polymers ($f=18$, asymmetric islands) investigated in the previous study and surprisingly similar to those with high functionality. This result indicates that linear chains ($f=2$) can collapse effectively because of their architecture, which allows low-density conformations under good solvent conditions. By contrast, at some critical number of arms, the constraint of the core leads to flatter/pancake-like conformations and increases the number of adsorbed monomers, thereby inhibiting a symmetric spherical cap formation and leading to asymmetry. However, at high functionality, the polymers start behaving like soft colloidal particles and symmetry returns. Second, the linear chain aggregates are spherical caps, whereas star polymer aggregates are asymmetric, which is attributed to the high osmotic pressure of star cores and the inability to fuse entirely; linear chains are easier to fuse into spherical cap-shaped nanodroplets.

Notably, the structures obtained with linear polymer suspensions spin-coated on weakly attractive substrates are less ordered, and they usually involve multichain nano/microdroplets of various sizes [47]. This comparison indicates the importance of long incubation under good solvent conditions, used in the present study, resulting in a uniform distribution of polymer chains.

CONCLUSIONS

Linear polymer (sub-)monolayers adsorbed on flat surfaces were studied by AFM. At sufficiently low surface densities, where the molecules can be considered isolated, the polymers adopt flat conformations. The height of the collapsed chains appeared almost independent of molecular weight. This behavior was due to the conformation of the isolated adsorbed chains when under good solvent conditions and before abrupt solvent evaporation. At high surface densities, aggregates of several polymer chains were formed for all molecular weights. Our results show that high-molecular-weight molecules can easily self-assemble into aggregates. This result has been explained on the basis of longer loops and tails of the high-molecular-weight chains. In most cases, at sufficiently high surface densities, an isotropic distribution of adsorbed polymers was observed, indicating near-to-equilibrium positions and conformations just before the sudden change of solvent conditions. A two-dimensional coarse-grained model based on the experimental observations was used to understand the aggregation effects. The simulations reproduced the experimental findings and further indicated that the conditions prior to the abrupt solvent evaporation determined the aggregation distribution after evaporation. The present study introduces a facile and inexpensive methodology for the manufacturing of hierarchical nanopatterns on surfaces based on the long molecular structures of polymers, the equilibration of the macromolecular system under good solvent conditions, and its abrupt transition to poor solvent conditions.

Acknowledgements

This work was supported by the EPSRC DTA and the Institute of Materials and Processes, School of Engineering at the University of Edinburgh. The authors are grateful to Jacques Roovers for the synthesis of the PB polymers. For the purpose of open access, the author has applied a Creative Commons Attribution (CC BY) licence to any Author Accepted Manuscript version arising from this submission.

Conflict of interest

The authors declare that they have no conflicts of interest.

References

1. Napper D. *Polymeric Stabilization of Colloidal Dispersions*. London: Academic Press; 1983.
2. Gast AP, Leibler L. Interactions of sterically stabilized particles suspended in a polymer solution. *Macromolecules*. 1986;19(3):686-91.
3. Berta M, Loppinet B, Vlassopoulos D, Askounis A, Koutsos V, Pastoriza-Santos I, et al. Tailoring the properties of grafted silver nanoprism composites. *Polymer*. 2012;53(25):5771-8. doi: <https://doi.org/10.1016/j.polymer.2012.10.034>.
4. Cox JK, Eisenberg A, Lennox RB. Patterned surfaces via self-assembly. *Current Opinion in Colloid and Interface Science*. 1999;4(1):52-9.
5. Cai J, Li C, Kong N, Lu Y, Lin G, Wang X, et al. Tailored multifunctional micellar brushes via crystallization-driven growth from a surface. *Science*. 2019;366(6469):1095-8. doi: [doi:10.1126/science.aax9075](https://doi.org/10.1126/science.aax9075).
6. Pugin R, Blondiaux N, Popa CT, Niedermann P, Liley M, Giazzon M, et al. Surface Nanopatterning by Polymer Self-Assembly: from Applied Research to Industrial Applications. *Journal of Photopolymer Science and Technology*. 2009;22(2):223-8. doi: [10.2494/photopolymer.22.223](https://doi.org/10.2494/photopolymer.22.223).
7. Pludeman E, Collins N. *Adhesion science and technology: [proceedings] (Polymer science and technology)*. New York: Plenum Press 1975.
8. Portigliatti M, Koutsos V, Hervet H, Léger L. Adhesion and Deformation of a Single Latex Particle. *Langmuir*. 2000;16(16):6374-6. doi: [10.1021/la000377i](https://doi.org/10.1021/la000377i).
9. McClements J, Koutsos V. Thin Polymer Film Force Spectroscopy: Single Chain Pull-out and Desorption. *ACS Macro Letters*. 2020;9(2):152-7. doi: [10.1021/acsmacrolett.9b00894](https://doi.org/10.1021/acsmacrolett.9b00894).
10. Migler KB, Hervet H, Leger L. Slip transition of a polymer melt under shear stress. *Physical Review Letters*. 1993;70(3):287-90.
11. Brown HR. Chain pullout and mobility effects in friction and lubrication. *Science*. 1994;263(5152):1411-3.
12. Léger L, Hervet H, Charitat T, Koutsos V. The stick–slip transition in highly entangled poly(styrene-butadiene) melts. *Advances in Colloid and Interface Science*. 2001;94(1):39-52. doi: [https://doi.org/10.1016/S0001-8686\(01\)00054-9](https://doi.org/10.1016/S0001-8686(01)00054-9).
13. De Gennes PG. Conformations of polymers attached to an interface. *Macromolecules*. 1980;13(5):1069-75.
14. Koutsos V, van der Vegte EW, Pelletier E, Stamouli A, Hadziioannou G. Structure of Chemically End-Grafted Polymer Chains Studied by Scanning Force Microscopy in Bad-Solvent Conditions. *Macromolecules*. 1997;30(16):4719-26. doi: [10.1021/ma961625d](https://doi.org/10.1021/ma961625d).
15. Koutsos V, van der Vegte EW, Hadziioannou G. Direct View of Structural Regimes of End-Grafted Polymer Monolayers: A Scanning Force Microscopy Study. *Macromolecules*. 1999;32(4):1233-6. doi: [10.1021/ma971702k](https://doi.org/10.1021/ma971702k).
16. Siqueira DF, Köhler K, Stamm M. Structures at the Surface of Dry Thin Films of Grafted Copolymers. *Langmuir*. 1995;11:3092-6.

17. Ross RS, Pincus P. Bundles - End-Grafted Polymer Layers in Poor Solvent. *Europhysics Letters*. 1992;19(2):79-84.
18. Yeung C, Balazs AC, Jasnow D. Lateral Instabilities in a Grafted Layer in a Poor Solvent. *Macromolecules*. 1993;26(8):1914-21.
19. Tang H, Szleifer I. Phase-Behavior of Grafted Polymers in Poor Solvents. *Europhysics Letters*. 1994;28(1):19-24.
20. Lai PY, Binder K. Structure and Dynamics of Polymer Brushes near the Theta Point - a Monte-Carlo Simulation. *Journal of Chemical Physics*. 1992;97(1):586-95.
21. Soga KG, Guo H, Zuckermann MJ. Polymer Brushes in a Poor Solvent. *Europhysics Letters*. 1995;29(7):531-6.
22. Grest GS, Murat M. Structure of Grafted Polymeric Brushes in Solvents of Varying Quality - a Molecular-Dynamics Study. *Macromolecules*. 1993;26(12):3108-17.
23. Williams DRM. Grafted Polymers in Bad Solvents - Octopus Surface Micelles. *Journal De Physique Ii*. 1993;3(9):1313-8.
24. Zhulina EB, Birshtein TM, Priamitsyn VA, Klushin LI. Inhomogeneous Structure of Collapsed Polymer Brushes under Deformation. *Macromolecules*. 1995;28(25):8612-20.
25. Sevick EM, Williams DRM. Polymers grafted onto strongly adsorbing surfaces in poor solvents: Stretching, fission, phase separation, and globular micelles in 2D. *Phys Rev Lett*. 1999;82(13):2701-4.
26. Fler GJ, Stuart MAC, Scheutjens JMHM, Cosgrove T, Vincent B. *Polymers at Interfaces*. Cambridge: Chapman & Hall; 1993.
27. Rubinstein M, Colby RH. *Polymer physics*. Oxford ; New York: Oxford University Press; 2003.
28. Haschke H, Miles MJ, Koutsos V. Conformation of a Single Polyacrylamide Molecule Adsorbed onto a Mica Surface Studied with Atomic Force Microscopy. *Macromolecules*. 2004;37(10):3799-803. doi: 10.1021/ma035881j.
29. Scheutjens J, Fler GJ. Statistical-Theory of the Adsorption of Interacting Chain Molecules .2. Train, Loop, and Tail Size Distribution. *Journal of Physical Chemistry*. 1980;84(2):178-90.
30. Semenov AN, Joanny JF. Structure Of Adsorbed Polymer Layers - Loops And Tails. *Europhysics Letters*. 1995;29(4):279-84.
31. Glynos E, Chremos A, Petekidis G, Camp PJ, Koutsos V. Polymer-like to Soft Colloid-like Behavior of Regular Star Polymers Adsorbed on Surfaces. *Macromolecules*. 2007;40(19):6947-58. doi: 10.1021/ma0708803.
32. Chremos A, Camp PJ, Glynos E, Koutsos V. Adsorption of star polymers: computer simulations. *Soft Matter*. 2010;6(7):1483-93. doi: 10.1039/b922988d.
33. Evangelopoulos AEAS, Glynos E, Madani-Grasset F, Koutsos V. Elastic Modulus of a Polymer Nanodroplet: Theory and Experiment. *Langmuir*. 2012;28(10):4754-67. doi: 10.1021/la2049037.
34. Evangelopoulos AEAS, Rissanou AN, Glynos E, Bitsanis IA, Anastasiadis SH, Koutsos V. Wetting Behavior of Polymer Droplets: Effects of Droplet Size and Chain Length. *Macromolecules*. 2018;51(8):2805-16. doi: 10.1021/acs.macromol.8b00033.
35. Roovers J, Toporowski P, Martin J. Synthesis and characterization of multiarm star polybutadienes. *Macromolecules*. 1989;22(4):1897-903. doi: 10.1021/ma00194a064.
36. Roovers J. Properties of the plateau zone of starbranched polybutadienes and polystyrenes. *Polymer*. 1985;26(7):1091-5. doi: [https://doi.org/10.1016/0032-3861\(85\)90234-4](https://doi.org/10.1016/0032-3861(85)90234-4).
37. Koutsos V, van der Vegte EW, Grim PCM, Hadziioannou G. Isolated Polymer Chains via Mixed Self-Assembled Monolayers: Morphology and Friction Studied by Scanning Force Microscopy. *Macromolecules*. 1998;31(1):116-23. doi: 10.1021/ma9706182.
38. Horcas I, Fernández R, Gómez-Rodríguez JM, Colchero J, Gómez--Herrero J, Baro AM. WSXM: A software for scanning probe microscopy and a tool for nanotechnology. *Review of Scientific Instruments*. 2007;78(1):013705.
39. Chremos A, Glynos E, Koutsos V, Camp PJ. Adsorption and self-assembly of linear polymers on surfaces: a computer simulation study. *Soft Matter*. 2009;5(3):637-45. doi: 10.1039/b812234b.

40. Louis AA, Bolhuis PG, Hansen JP, Meijer EJ. Can Polymer Coils Be Modeled as “Soft Colloids”? *Physical Review Letters*. 2000;85(12):2522-5.
41. Allen MP, Tildesley DJ. *Computer Simulation of Liquids* Oxford: Clarendon Press; 1987.
42. Kiriy A, Gorodyska G, Minko S, Jaeger W, Stepanek P, Stamm M. Cascade of coil-globule conformational transitions of single flexible polyelectrolyte molecules in poor solvent. *Journal of the American Chemical Society*. 2002;124(45):13454-62.
43. Minko S, Kiriy A, Gorodyska G, Stamm M. Single flexible hydrophobic polyelectrolyte molecules adsorbed on solid substrate: Transition between a stretched chain, necklace-like conformation and a globule. *Journal of the American Chemical Society*. 2002;124(13):3218-9.
44. Gorodyska G, Kiriy A, Minko S, Tsitsilianis C, Stamm M. Reformation and metallization of unimolecular micelles in controlled environment. *Nano Letters*. 2003;3(3):365-8.
45. Luzinov I, Minko S, Tsukruk VV. Adaptive and responsive surfaces through controlled reorganization of interfacial polymer layers. *Progress in Polymer Science*. 2004;29(7):635-98.
46. Thiele U, Mertig M, Pompe W. Dewetting of an evaporating thin liquid film: Heterogeneous nucleation and surface instability. *Phys Rev Lett*. 1998;80(13):2869-72.
47. McClements J, Buffone C, Shaver MP, Sefiane K, Koutsos V. Poly(styrene-co-butadiene) random copolymer thin films and nanostructures on a mica surface: morphology and contact angles of nanodroplets. *Soft Matter*. 2017;13(36):6152-66. doi: 10.1039/C7SM00994A.